RSC Advances

ROYAL SOCIETY OF CHEMISTRY

www.rsc.org/advances

Journal Name

RSCPublishing

COMMUNICATION

High Performance Mesoporous C@Se Composite Cathodes Derived from Ni-based MOFs for Li-Se Batteries

Cite this: DOI: 10.1039/x0xx00000x

Ting Liu[a,b†], Yan Zhang [a,b], Junke Hou [a,b], Shiyu Lu[a,b], Jian Jiang[a,b], Maowen Xu[a,b*†]

Received 00th January 2012,
Accepted 00th January 2012

DOI: 10.1039/x0xx00000x

www.rsc.org/

A mesoporous carbon matrix derived from MOF-Ni prepared via hydrothermal method was used for encapsulating selenium as cathode material for Li-Se batteries. Thermogravimetric analysis and energy-dispersive X-ray analysis confirm that selenium is highly homogeneous distributed in the composite with a mass loading up to 48%. It exhibits an initial discharge capacity of 599.7 mA h g^{-1} and retains 417 mA h g^{-1} with a high Coulombic efficiency of 99.9 % after 100 cycles at a high rate of 3C, of which the excellent electrochemical performance is mainly attributed to the high conductivity and the hollow structure of carbon matrix.

1. Introduction

At present, in order to meet the increasing demand for development of mobile devices and hybrid electric vehicles which have exacting requirements on battery volume, thus thoroughly improving the properties of high capacity energy storage system appears to be imperative[1,2]. Among all the advanced next-generation lithium battery systems, lithium-sulfur (Li-S) batteries, due to its outstanding high theoretical specific capacity (1672 mAh g^{-1}) and energy density (2600 Wh Kg^{-1}), have become a research focus beyond other secondary power batteries recently [3]. However, its large-scale industrial application is still hampered because of low electronic conductivity of elemental S and the shuttle effect caused by dissolving of high-order polysulfide in organic electrolyte [4].

Therefore, it is vital to explore and develop new cathode materials with excellent electric conductivity and cyclic stability which could further implement high capacity and long cycle life. Elemental selenium (Se) would be a promising candidate as cathode material. On the one hand, as a congener of element S, Se is provided with a similar electrochemical performance to S, and its reaction with metallic lithium can be described as follows [5]:

$$Se + 2Li^+ + 2e^- \longleftrightarrow Li_2Se$$

On the other hand, as a semiconductor, Se displays much higher electric conductivity than that of S, nearly 20 orders of magnitude (1×10^{-3} S m^{-1} vs. 5×10^{-28} S m^{-1}) [6], which makes it possible for its good electrochemical activity and greatly improved efficiency, and finally can lead to fast charging and discharging process. Moreover, Se possesses comparatively high density and two-electron reaction mechanism during delithiation-lithiation processes, resulting in a high theoretical volumetric capacity (3253 mAh cm^{-3} -based on 4.82 g cm^{-3}), which makes up for its relatively low theoretical gravimetric capacity (675 mAh g^{-1}) to S cathode [7,8]. Herein, Li-Se batteries has the prospect of becoming another high-profile battery system after Li-S batteries. However, poor cycle life is always the biggest hindrance toward the commercialization of Li-S as well as Li-Se batteries. In order to avoid fast fading of capacity and poor performance of Coulombic efficiency, much effort has been made [9]. One efficient solution is compositing porous carbon materials with S/Se, for that their conductive network is found to be effective to improve electrical

conductivity of S/Se, and thereby reduce the dissolution of polysulfide, besides, they can provide an unhindered electronic channel, and also can alleviate the change of volume as a buffer layer [10].

Lately, metal organic frameworks (MOFs) have attracted much attention and gotten extensive recognition because of their special porous structure. After carbonization, they can be widely employed in super capacitor electrodes[11], sensing[12], hydrogen evolution[13] and Li-S batteries[14] due to excellent features including large specific surface area, high porosity, adjustable pore diameter size, high structural plasticity, etc. By means of selecting different metals and organic-ligands, it would be convenient to prepare various carbon materials with required pore shape, size and volume, which forebodes that MOFs-derived carbon materials could be widely used in Se cathode. Guo generated an advanced selenium-carbon cathode by confining Se_8 molecules in ordered mesopores of CMK-3, exhibiting good electrochemical performance[15].Lai et al. [16] used Se confined in mesoporous carbon matrix derived from MOF-5 as cathode material, and found that meso-C@Se cathode has great cycling stability, coulombic efficiency and high rate performance. Nitrogen-doped carbon rod-like sponge (NCS) derived from one kind of Al-MOF is used to confine Se as cathode material by Li et al. [17].

In this study, we chose metal nickel and terephthalic acid (PTA) as ingredient to prepare MOF-Ni precursor via traditional hydrothermal method. Mesoporous carbon material derived from MOF-Ni by means of high temperature calcination was mixed with selenium powder uniformly through wet grinding. The as-prepared meso-C@Se cathode delivers a high reversible capacity, good rate capability and long-term cycling stability.

2. Experimental

2.1.Synthesis of meso-C@Se composite

All chemicals were purchased from Sigma Aldrich and used as received. In a typical procedure, terephthalic acid (PTA) (0.237 g) was dissolved in N, N-dimethylformamide (DMF) (15 mL) under constantly stirring, meanwhile, $NiCl_2 \cdot 6H_2O$ (0.51g) was dissolved in 20 mL of deionized water. Then the nickel chloride aqueous solution was added to the organic solution drop by drop followed by continually stirring for 1h. The mixture was then directly transformed into a Teflon-lined stainless steel autoclave with a capacity of 35 ml, and was kept at 120 ℃ for 12 h. After cooling to room temperature, the resulting precipitate was filtered and washed with DMF and alcohol for several times. At last, the crystals were dried in air at 70 ℃ for 12 h, and the light green powder was exactly Ni-based MOF materials.

Meso-C was obtained via one-step pyrolysis of MOF-Ni. To pyrolyze the organic species, MOF-Ni was transferred to a tube furnace and was heat-treated at 800 ℃ for 3 h under nitrogen atmosphere with a heating rate of 5 ℃ min^{-1}. After cooling down, MOF-Ni was successfully transformed into porous carbon. Then, a mixture of meso-C and selenium powder with mass ratio of 1:2 were wet grinded with ethanol in an agate mortar for 30 min. After thoroughly dry, the mixture was heated at 260 ℃ for 20 h.

2.2. Characterization of materials

The morphologies analyses were observed with field emission scanning electron microscopy (FESEM, JSM-7800F, Japan). The structure analyses were recorded by powder X-ray diffraction (XRD, MAXima-X XRD-7000). X-ray photoelectron spectroscopy (XPS) measurements were performed on a Thermo Scientific ESCALAB 250Xi electron spectrometer. Fourier transform-infrared (FT-IR) spectra were characterized on the Nicolet FTIR 6700 spectrophotometer (Thermo Nicolet). In terms of specific surface area and pore size distribution of the MOF-Ni, moso-C and meso-C@Se were determined by Brunauer–Emmett–Teller (BET) method using an ASAP-2010 surface area analyzer. The content of Se in meso-C@Se was measured by Thermo Gravimetric Analyzer (TGA, Q50, USA) under N_2 atmosphere.

2.3 Electrochemical measurements

The working electrode was prepared by a slurry coating procedure. The cathode slurry consisted of 80 wt% active material (meso-C@Se composite), 10 wt% carbon black (Super P, Timcal) and 10 wt% water-soluble binder sodium alginate ($(C_6H_7O_6Na)_n$, SA), using SA and water replace conventional polyvinylidene fluoride (PVDF) and N-methyl pyrrolidone (NMP), therefore reflects a cleaner production technology. Then, the slurry was uniformly cast on an etched aluminum foil current collector using a doctor blade technology. The pristine selenium

cathode CB@Se containing 60 wt% Se, 40 wt% carbon black and 10 wt% SA binder was prepared by the same way for comparison. Finally, the electrodes were dried under vacuum at 60 ℃ for 24 h to remove the solvent.

Test cells were assembled in an Ar-filled glove box (Dellix-LS800S, Dellix Industry Co., LTD, China) under the condition that oxygen and water contents were less than 1 ppm. In 2032-type coin cells, we use meso-C@Se composite as the cathode, while Li foil as the counter as well as reference electrode, and microporous polypropylene (PP) film as the separator. During the process, 1 M bis (trifluoromethane) sulfonamide lithium salt (LiTFSI, Sigma Aldrich) and 0.1 M $LiNO_3$ in a mixed solvent of 1, 3-dioxolane (DOL, Sigma Aldrich) and 1, 2-dimethoxyethane (DME, Sigma Aldrich) with a volume ratio of 1: 1 was used as the electrolyte.

All the experiments were conducted at room temperature. The coin cells were galvanostatically charged–discharged at desired current densities between 1.0 and 3.0 V (vs. Li/Li^+) on a Land cycler (Wuhan Kingnuo Electronic Co., China). Cyclic voltammetry (CV) test was conducted using a CHI 660c electrochemical workstation (Shanghai Chenhua, China) at a scan rate of 0.1 mV s^{-1} in the voltage range from 1.0 to 3.0 V.

3. Results and discussion

3.1. Synthesis and structural analysis of meso-C@Se composite

Fig.1a shows the XRD patterns of meso-C as well as meso-C@Se, which clearly reveals the lattice structure and chemical composition of the sample. For meso-C, the characteristic peak of carbon appear at around 26°, other three sharp peaks belong to residue of nickel (PDF#70-0989), whose existence might improve the conductivity. There is no characteristic peak of pure Se in the pattern of the meso-C@Se composite , showing the most of Se exist in amorphous state, and those diffraction peaks belong to $NiSe_2$ (JCPDS41-1495). The XRD patterns of MOF-Ni is displayed in Fig. S2., there are three sharp peaks at 2θ=9.3, 11.8, 23.8, fitting very well with the corresponding lattice planes of (100), (010) and (020), respectively. It is standard XRD pattern (CCDC No. 638866, space group: *P-1*) that in good accordance with our experiment result.

To figure out what functional groups did the MOF-Ni contain, FT-IR test was performed. As shown in Fig.1b, the stretching vibration of para-aromatic CH groups is reflected at ~1501 cm^{-1}, while the stretching vibration of OH^- appears at ~3586 cm^{-1}. Meanwhile, the stretching vibration bands around 3051, 3338 and 3421 cm^{-1} belong to H_2O molecules, proving the existence of coordinated H_2O molecules in the as-prepared MOF-Ni. At ~1375 and ~1568 cm^{-1}, there are two intensive bonds that should be attributed to the asymmetric and symmetric stretching modes of the coordinated group ($-COO^-$). Being in agreement with the XRD pattern, the separation between the above two modes demonstrates successful coordination between $–COO^-$ from PTA and Ni^{2+} via a bidentate mode. As for FT-IR spectrums of meso-C and meso-C@Se, they are coincident with each other, strongly suggesting the structure stability of the matrix. The crystal structure of the as-prepared MOF-Ni and its TGA curve are displayed in Fig.S1.(Supplementary Fig.S1.), demonstrating a weight loss of 63% after the high temperature heating of 800 ℃.

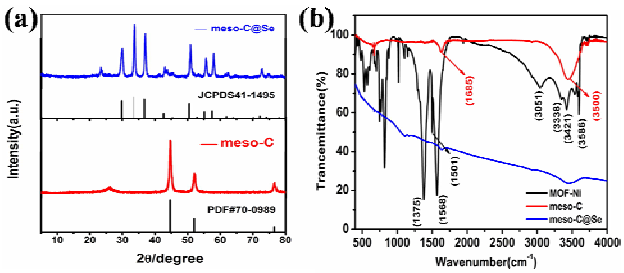

Fig. 1. (a) XRD patterns of meso-C derived MOF-Ni and the meso-C@Se composite; (b) FT-IR spectrums of the MOF-Ni and meso-C derived MOF-Ni as well as the meso-C@Se.

The morphology of the precursor MOF-Ni was investigated by FESEM. It turns out to be a parallelogram-like shape with micron size and smooth surface (Fig.2a), and small cracks can be seen on the surface in Fig.2b.

In terms of morphology of the obtained meso-C material, it kept the original parallelogram square brick structures with numerous mesopores on the surfaces, as shown in Fig.2c, d. Fig.2e and f display the structural change after impregnating Se into the meso-C, and we find the difference between the FESEM images of meso-C and meso-C@Se is that there is no bulky particles on the surface of meso-C@Se, making clear the successful impregnation of Se into the meso-C [16].

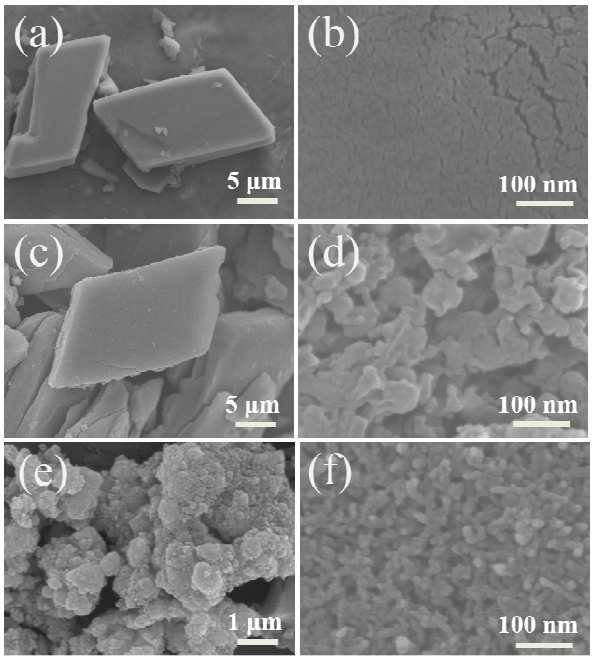

Fig. 2. FE-SEM images of MOF-Ni (a), (b); meso-C derived MOF-Ni (c), (d); and meso-C@Se (e), (f) under the low and high magnification rate.

Through the adoption of energy dispersive X-ray spectroscopy (EDS) analysis, whose result is shown in Fig.3b, c and d, it can be seen that elemental mapping of C, Se, and Ni presents a homogeneous distribution in meso-C@Se, which is a huge vindication that Se was confined in the pore of meso-C.To further confirm the elements in meso-C, EDS analysis are displayed in Fig.S3.(Supplementary Fig.S3.), there are numbers of microspheres can be seen embedded thoroughly and are clear at a glance to be judged as residual Ni^{2+}, whose amount is confirmed by line scanning result of EDS in Fig.S4.

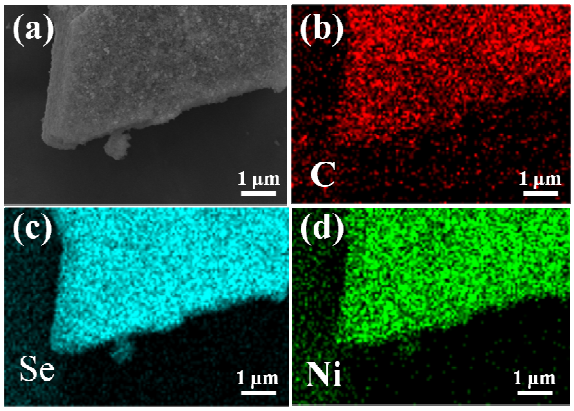

Fig. 3. Elemental mappings of carbon(b); and selenium(c) ; and nickel(d) in meso-C@Se.

Further illustrating the elements that meso-C@Se composite contained, XPS is employed to characterize the chemical composition and chemical bonding state of the composite. In Fig.4a, C1s spectra is well behaved, the appearance of carboxyl bonds may be caused by incomplete carbonation. For Fig.4b, the Se 3d spectrum is fitted into two peaks at 55.6 and 54.4 eV are assigned to Se 3d 3/2 and Se 3d 5/2 on the account of spin orbit coupling[18]. In addition to the normal two peaks, there is one more peak at 58.8 eV, which may come from the Se–Se bonds located at the chain end of the chain-like Sen molecules since they possess higher binding energy than the normal ones. Other cause may be Se anions reacted with carbonyl groups during the heating treatment thus produced Se-C and/or Se-O bonds. Therefore, the mentioned three bonds may all contribute to the new peaks [19].

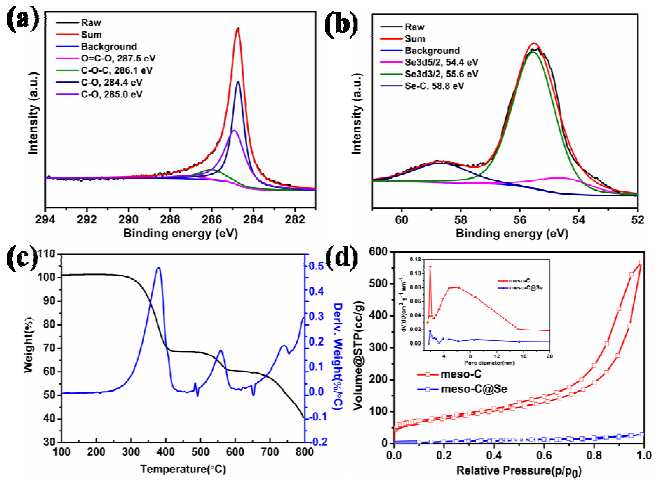

Fig.4. (a) XPS spectra of C 1s, (b) Se 3d of meso-C@Se; (c) TGA curve of meso-C@Se composite; (d) N_2 adsorption–desorption isotherms and mesopore size distribution of meso-C and meso-C@Se composite.

Since weight loss is mostly derived from the Se evaporation, the thermogravimetric pattern is also a strong evidence of Se absorption strength in carbon mesopores[20]. Therefore, thermogravimetric analysis (TGA) was performed in N_2 flow to confirm the content of Se and the mechanism of Se confinement in meso-C@Se. As is shown in Fig.4c, total weight loss of approximately 60% occurs during the heat treatment for the meso-C@Se sample. However, there are three evaporation peaks shown in Fig. 4c, only the first two belong to Se evaporation, the last one may due to the decomposition of the material or the evaporation of $NiSe_2$. The peak at 400 ℃ is attributed to Se that evaporated from surface which is similar to previous studies [21,

[22]. The other peak at 550 ℃ corresponds to Se that evaporated from internal hollow structure of meso-C. A higher evaporation temperature indicates that Se molecules hosted in internal hollow structure are more difficult to remove than those on surface. The two-step mass loss of the sample accounts for 48 wt% Se in the meso-C@Se composite, corresponding to the result of line scanning shown in Fig.S4. From what has been discussed above, the content of mesoporous carbon can be identified as 42 wt% in the composite.

Fig.4d exhibited the N_2 adsorption-desorption isotherms of meso-C and meso-C@Se, from which we can transparently see the change of specific surface area of them. The meso-C material own a nearly 300 m^2 g^{-1} specific surface area and a 0.856 m^3 g^{-1} pore volume, both of them decreased notably after Se loading, that the specific suface area of meso-C@Se composite is about 26.4 m^2 g^{-1} and the pore volume is 0.041 m^3 g^{-1}. The image of pore size distribution of meso-C and meso-C@Se composite is embedded in Fig.4d in the top left corner. Meso-C sample exhibits a bimodal pore size distribution mainly in the region of mesopore (4–15 nm), indicating abundant mesoporosity structure in the meso-C material. It is found that the pore size distribution of meso-C in mesopore region (4–15 nm) reduces sharply after Se insertion, the result is in accordance with the decreases of specific suface area and pore volume, which suggests that Se was successfully implanted into meso-C.

3.2. Electrochemical characterization

For the purpose of figuring out the oxidation/reduction reactions in Li-Se batteries, the initial three consecutive cyclic voltammograms(CVs) of the meso-C@Se composite are shown in Fig.5a. It shows two obvious reduction peaks at around 1.94 V and 2.14 V in first cycle, corresponding to two step reaction of elemental Se with metallic Li during the discharge process: Se to high-order soluble polyselenides Li_2Se_n ($n \geq 4$) and further reduction to the insoluble Li_2Se_2 and Li_2Se[8]. In the meantime, only one single oxidation peak at 2.25 V is observed during the whole anodic scan process, which can be attributed to the delithiation process of Li_2Se switching to soluble polyselenides[23]. The CV curves overlap well with each other, demonstrating a good cycling stability during the subsequent cycles and indicating that the hollow carbon structure is quite effective in preventing the loss of selenium into the electrolyte and improving coulombic efficiency[24].

To evaluate the lithium storage properties of the meso-C@Se samples, galvanostatic charge-discharge experiments were carried out at a current density of 2 C (1350 mA g^{-1}) in the voltage range between 1.0 V and 3.0 V at 25 □. Fig.5b displays the charge/discharge profiles for different cycles at 1st, 5 th, 10 th, 20 th, 50 th, 100 th and 500 th of meso-C@Se composite. Two typical discharge potential plateaus at 1.94 V and 2.14 V are generally corresponding to the result of CV measurement, which is a vivid portrayal of the reaction between elemental Se and metallic Li during the discharge process. In the first cycle, the initial discharge capacity reaches up to 719.7 mA h g^{-1}, while the charge capacity is 760.1 mA h g^{-1}. Note that with the increase of cycle number, the capacity of meso-C@Se cathode decreases slowly, the discharge/ charge profiles of 5th, 10th, 20th, 50th, and 100th overlap with each other to a great extent. After 100 cycles, the discharge capacity of the Se cathode can still retain 435.7 mA h g^{-1}. Even after 500 cycles, the reversible capacity is still more than 250 mA h g^{-1}, indicating a fairly stable electrochemical performance of meso-C@Se composite cathode and further determining its relatively high stability and reversibility.

Cycling performance and Coulombic efficiency of the meso-C@Se composite cathode are displayed in Fig.5c at a current density of 3 C (2025 mA g^{-1}). With the initial discharge capacity of 599.7 mA h g^{-1}, the cathode exhibits a high utilization of active materials. For comparison, cycling performance of CB@Se is presented in Fig. S5 (b), in which the pristine Se cathode shows the initial discharge capacity of 525.3 mAh g^{-1} at 3 C(1350 mA g^{-1}). Even after 100 cycles, the reversible capacity of meso-C@Se retains 417.3 mA h g^{-1}, which is approximately five times than the CB@Se cathode whose reversible capacity is only 83.6 mAh g^{-1}, demonstrating the great improvement in specific capacity as well as capacity retention of meso-C@Se composite. The good conductivity of meso-C provides a faster Li^+ diffusion pathway, not only does this host material show stronger constraint ability for Se, but also effectively inhibits the shuttle reaction, thus contributing to higher reversible capability of the meso-C@Se composite cathode.

As for the Coulombic efficiency of the meso-C@Se composite cathode, it reaches up to 99.25 % after the third cycle, though it shows a slow decrease in the first ten cycles, finally reaching 473.5 mA h g^{-1} with a Coulombic efficiency of 97.64 % at the 10th cycle, it increases to nearly 100 % after 100 cycles and lasts to the 500th cycle. During 20th to 100th cycle, it shows

perfect stability with only about 0.23 % capacity loss per cycle. The stable maintaining of Coulombic efficiency reflects from one point that the mespore structure is effective in suppressing the dissolution of polyselenides into the electrolyte and in maintaining high utilization of the active materials during the charge/discharge process.

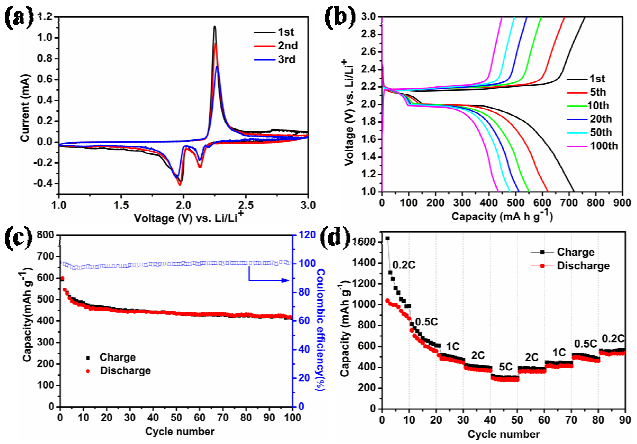

Fig.5. (a) CV curves of the meso-C@Se cathode for three cycles at a scan rate of 0.1 mV s^{-1} in the voltage range of 1.0-3.0 V; (b) Discharge−charge profiles of the meso-C@Se cathode at a current density of 3 C in the voltage range of 1.0-3.0 V; (c) Cycling performance of meso-C@Se composites at 3 C, blue circles showing the Coulombic efficiency of meso-C@Se; (d) Rate capabilities of meso-C@Se composites.

Rate capability is one of the essential parameters for high energy batteries. The rate capacity of the meso-C@Se composite was tested to get further insight into the improved electrochemical performance of the cathode. Being shown in Fig.5d, the cells were charged/ discharged with different C-rates at 0.2 C, 0.5 C, 1 C, 2 C and 5 C for 10 cycles each and then reverted to 0.2 C for endurance test. Due to the instability at the beginning, the initial discharge capacity reaches up to 1038.9 mAh g^{-1}. After 10 cycles at a current density of 0.2 C (135 mAh g^{-1}), meso-C@Se composite cathode shows the reversible capacity of 866.9 mAh g^{-1} which is higher than the previous report[22]. At 0.5 C (337.5 mA h g^{-1}), the reversible specific capacity can remains at values of 555 mA h g^{-1}, which is over double of the previous research results[24]. Even after 50 cycles at a higher current density of 5 C (3375 mA h g^{-1}), the cathode displays good reversible capacity of 281.2 mA h g^{-1}. Until 90 cycles, as the current density returns to 0.2 C, the reversible specific capacity can remains at values of 517.2 mA h g^{-1}, while pristine Se cathode that only maintains the reversible capacity of 103.8 mAh g^{-1} according to the report of Lai et al[16]. To be sure, the MOF-Ni derived meso-C@Se composite cathode greatly improved the rate performance of pristine Se cathode. Both the outstanding cycling performance and rate capability of the as-prepared meso-C@Se composite should be given credit to the unique porous structure and good electronic properties of MOF-Ni derived meso-C material. It is the hollow structure that results in uniform dispersion of Se and accommodates the volume change during the electrochemical reactions.

4. Conclusions

In summary, we have successfully synthesized MOF-Ni, a porous metal organic framework, by a one-step hydrothermal synthesis method. Then it was used as a precursor to obtain meso-C via carbonization treatment followed by confining Se in the hollow of mesoporous texture carbon by a facile melt-diffusion route. Used as cathode for rechargeable Li–Se battery for the first time, the meso-C@Se composite exhibits stable cycling performance, high Coulombic efficiency and excellent rate capability. All of the test results reveal that Se-based cathode material will have a broad developing prospect in the application of future rechargeable lithium batteries.

Acknowledgements

This work is financially supported by Chongqing Key Laboratory for Advanced Materials and Technologies of Clean Energies under cstc2011pt-sy90001, Start-up grant under SWU111071 from Southwest University and Chongqing Science and Technology Commission under cstc2012gjhz90002. The work is supported by grants from Fundamental Research Funds for the Central Universities (SWU 113079, XDJK2014C051).

Notes and references

[a]*Institute for Clean Energy & Advanced Materials, Faculty of Materials and Energy， Southwest University, Chongqing 400715, P.R. China*

[b]*Chongqing Key Laboratory for Advanced Materials and Technologies of Clean Energies, Chongqing 400715, P.R. China*

Fax: +86-23-68254969; Tel: +86-23-68254969;

E-mail: xumaowen@swu.edu.cn

[1] M. Armand, J. M. Tarascon, *Nature*, 2008, **451**, 652-657.

[2] G. He, S. Evers, X. Liang, M. Cuisinier, A. Garsuch, L. F. Nazar, *ACS nano*, 2013, **7**, 10920.

[3] Z. Liang, G. Zheng, W. Li, Z.W. Seh, H. Yao, K. Yan, D. Kong, Y. Cui, *ACS nano*, 2014, **8**, 5249.

[4] Y.X. Yin, S. Xin, Y.G. Guo, L.J. Wan, *Angewandte Chemie-International Edition*, 2013, **52**, 2.

[5] L. L. Liu, Y. Y. Hou, X. W. Wu, *Chem Commun*, 2013, **49**, 11515-11517.

[6] A. Abouimrane, D. Dambournet, K. W. Chapman, P. J. Chupas, W. Weng, K. Amine, *J. Am. Chem. Soc.*, 2012, **134**, 4505–4508.

[7] K. Han, Z. Liu, H. Ye, F. Dai, *J. Power Sources*, 2014, **263**, 85.

[8] Y. Cui, A. Abouimrane, J. Lu, T. Bolin, Y. Ren, W. Weng, C. Sun, V. A. Maroni, S. M. Heald, K. Amine, *J. Am. Chem. Soc.*, 2013, **135**, 8047–8056.

[9] J. Kim, D. J. Lee, H. G. Jung, Y. K. Sun, J. Hassoun, B. Scrosati, *Adv. Funct. Mater*, 2013, **23**, 1076-1080.

[10] S. Jiang, Z. Zhang, Y. Lai, Y. Qu, X. Wang, J. Li, *J. Power Sources*, 2014, **267**, 394-404.

[11] W. Chaikittisilp, M. Hu, H. Wang, H. S. Huang, T. Fujita, K. C. Wu, L. C. Chen, Y. Yamauchi, K. Ariga, *Chem Commun (Camb)*, 2012, **48**, 7259-7261.

[12] M. Hu, J. Reboul, S. Furukawa, N. L. Torad, Q. Ji, P. Srinivasu, K. Ariga, S. Kitagawa, Y. Yamauchi, *J Am Chem Soc*, 2012, **134**, 2864-2867.

[13] H. L. Jiang, B. Liu, Y. Q. Lan, K. Kuratani, T. Akita, H. Shioyama, F. Zong, Q. Xu, *J. Am. Chem. Soc.*, 2011, **133**, 11854-11857.

[14] K. Xi, S. Cao, X. Peng, C. Ducati, R. V. Kumar, A. K. Cheetham, *Chem Commun (Camb)*, 2013, **49**, 2192-2194.

[15] C. Yang, S. Xin, Y. Yin, H. Ye, J. Zhang, Y. Guo, *Angew Chem Int Ed Engl*, 2013, **52**, 8363-8367.

[16] Y. Q. Lai, Y. Q. Gan, Z. Zhang, W. Chen, J. Li. *Electrochimica Acta*, 2014, **146**, 134–141.

[17] Z. Q. Li, L. W. Yin, *Nanoscale*, 2015, **7**, 9597–9606.

[18] H Ye, Y. X. Yin, S. F. Zhang, Y. G. Guo, *J. Mater. Chem. A*, 2014, **2**, 13293–13298.

[19] Z. Li, L. X. Yuan, Z. Q. Yi, Y. Liu, Y. H. Huang, *Nano Energy*, 2014, **9**, 229-236.

[20] J. Guo, Y. Xu, C. Wang, *Nano Lett*, 2011, **11**, 4288-4294.

[21] C. Luo, Y. Xu, Y. Zhu, Y. Liu, S. Zheng, Y. Liu, A. Langrock, C. Wang, *ACS Nano*, 2013, 7, 8003-8010.

[22] H, Ye, Y. X. Yin, S. F. Zhang, Y. G. Guo, *J. Mater. Chem. A*, 2014, **2**, 13293.

[23] Z. Zhang, X. Yang, X. Wang, Q. Li, Z. Zhang, *Solid State Ionics*, 2014, **260**, 101.

[24] J. Li, X. X. Zhao, Z. Zhang, Y. Q. Lai. *J. Alloys. Compd.*, 2015, **619**, 794–799.

[25] Z. Zhang, X. Yang, Z. P. Guo, Y. H. Qu, J. Li, Y. Q. Lai, *J. Power Sources*, 2015, **279**, 88-93.